Transmission electron microscope observations of planar defects in ferrierite from Kamloops Lake, British Columbia

STEPHEN B. RICE

McCrone Associates, Incorporated, 850 Pasquinelli Drive, Westmont, Illinois 60559, U.S.A.

ABSTRACT

Transmission electron microscope images of the zeolite ferrierite, prepared by ultramicrotomy as cross sections of the main-channel axis, revealed several types of crystallographic defects. Both shear faults and sigma transformations occur in the vug-filling bundles of ferrierite near Kamloops Lake, British Columbia. Sigma contraction {110} planes occur as discrete domains several unit cells thick. Shear faults involving displacements of $(a \pm b)/2$ on {110} planes occur in lesser amounts. In addition, mordenite occurs in the Kamloops Lake sample, underscoring the frequent association of these zeolites, their crystal chemical and structural affinities, and the importance of TEM-scale observations in petrologic studies of fine-scale intergrowths of zeolites.

INTRODUCTION AND BACKGROUND

The subject of defects in zeolites is important for understanding the rich diversity in mineral behavior and the potential for industrial catalytic and separations applications of these minerals. Defects in ferrierite are no exception. Ferrierite is an uncommon zeolite, having been recognized in fewer than 30 occurrences worldwide. Although exploitation of natural zeolite deposits for catalysis is hindered by impurities, study of zeolite mineralogy provides insight into some of the chemical and physical properties relevant for their application. Increased attention to synthetic ferrierite for use in the petrochemical industry motivated the present study. Previous microscopy studies of ferrierite (Gramlich-Meier et al., 1984; Sanders, 1985; Smith, 1986) concentrated on inferences from selected-area electron diffraction (SAED) patterns because of difficulties in obtaining high-resolution TEM (HRTEM) images of these beam-sensitive materials. Preliminary TEM studies on ferrierite from the Lovelock deposit indicated that several distinct types of defects occur (Rice et al., 1990). Smith (1986) presented some images parallel to [100] that did not show defects at high resolution. A recent modeling study of powder X-ray (XRD) and electron diffraction data for Lovelock ferrierite (Rice et al., 1994) indicated that they are consistent with $c/2$ shear faults primarily on (040) and secondarily on (400). Sigma transformations (Shoemaker et al., 1973) could not explain the data.

The present study of ferrierite was initiated to image directly the ferrierite framework close to the [001] axis and to confirm the presence of planar defects. The Kamloops Lake ferrierite occurs in bundles of radiating prismatic crystals. To obtain electron micrograph views parallel to the c-axis ten-membered ring channels, ultramicrotomed thin sections of oriented fibers were made. If, as hypothesized by Gramlich-Meier et al. (1984),

sigma transformations contribute significantly to the streaking observed in SAED patterns, the [001] projection should reveal such faults.

Ferrierite crystal chemistry

Ferrierite was first reported by Graham (1918) as a vug-filling mineral associated with chalcedony and calcite in altered olivine basalt near Kamloops Lake, British Columbia. Since then, nearly 30 ferrierite occurrences have been reported worldwide. The crystal structure was determined by single-crystal X-ray structure refinements on crystals from Kamloops and simultaneously reported by Vaughan (1966) and Kerr (1966). It has orthorhombic symmetry, space group *Immm,* and unit-cell parameters $a = 1.92$, $b = 1.41$, and $c = 0.75$ nm. Ferrierite is classified structurally as a member of the mordenite group (Gottardi and Galli, 1985), which includes mordenite, ferrierite, epistilbite, bikitaite, and dachiardite. Intersecting ten-membered ring (0.55 nm) and eight-membered ring (0.43 nm) channels parallel to c and b, respectively, characterize the channel system of ferrierite (Fig. 1) and make it a potentially very interesting molecular sieve and catalyst. Mordenite has twelve-membered ring channels, with a free diameter of about 0.7 nm. The recently discovered zeolite boggsite (Pluth and Smith, 1990), the first to contain intersecting ten- and twelve-membered ring channels, has a ten-membered ring projection similar to ferrierite.

The chemical composition for ferrierite is approximately $(Na,K)Mg_2Ca_{0.5}(Al_6Si_{30}O_{72}) \cdot 18H_2O$. The framework composition is restricted to between Al_5Si_{31} and $Al_{8.5}Si_{27.5}$ (Wise and Tschernich, 1976), but the exchangeable cation composition is quite variable. As with many zeolite structures, exchangeable cation positions in ferrierite are not completely known. The Na^+ ions in ferrierite are probably located in the main (ten-membered

ring) channels (Vaughan, 1966). The only cation located with certainty in structure refinements is Mg, which is coordinated by six H_2O molecules occupying six-membered ring cages. Alberti and Sabelli (1987) refined the crystal structure of the ferrierite from Monastir, Sardinia, in space group *Immm*. They argued that one of the bridging O angles (T4-O5-T4) is constrained to 180° in *Immm* and that the true, lower symmetry does not require this energetically unfavorable configuration. They also noted that the true symmetry of the $Mg(H_2O)_6^{2+}$ octahedron within the six-membered ring cage suggests a lower symmetry consistent with the subgroup *Pnnm*. A monoclinic variety of ferrierite was reported by Gramlich-Meier et al. (1985). This particular specimen has low Mg (~ 1 Mg/unit cell), which permits the six-membered ring cages to collapse and distort, thus producing monoclinicity.

Although Graham (1918) also found {010} and {101} forms, the habit of ferrierite in vug occurrences, such as at Kamloops Lake, is predominantly prismatic needles parallel to [001], often in bundles radiating from a common point. Ferrierite with prismatic habit occurs commonly in the Lovelock deposit (Rice et al., 1992), but in much smaller proportions than the laths. Perfect cleavage occurs parallel to {100} planes, a behavior readily understood from the crystal structure. Unfortunately, images in this direction provide the least information about the proposed defects. The [001] and [010] views are difficult to obtain in dispersion preparations, which is why sections were made in the present study.

Types of defects in ferrierite

Sigma faults. The sigma transformation is a mechanism proposed by Shoemaker et al. (1973) and consists of the insertion or removal of planes of tetrahedra in a zeolite framework, often at positions of mirror symmetry. In ferrierite, planes of Si and Al tetrahedra normal to [010] could be added or removed, causing the structure (and, particularly, the ten-membered rings) to expand or to contract (Fig. 2). Expansion causes the ten-membered rings to become twelve-membered and the six-membered rings to become eight-membered, whereas contraction causes the ten-membered rings to become eight-membered and the six-membered rings to become four-membered. In the contraction case, the five-membered rings become distorted six-membered rings. Clearly, a large number of faults changes the sieving and exchange properties of the material but does not affect the [010] projection (Fig. 2B).

An analogous set of sigma faults on the {110} planes would have the same relative size effects on the ten-membered ring channels and the six-membered ring apertures. However, there are some differences between these and (010)-type sigma transformations. The contraction fault on (110) planes results in a displacement of $c/2$, offsetting the eight-membered ring channels (Fig. 2D), whereas the expansion fault requires no such displacement. Furthermore, with expansion, four-membered rings are created
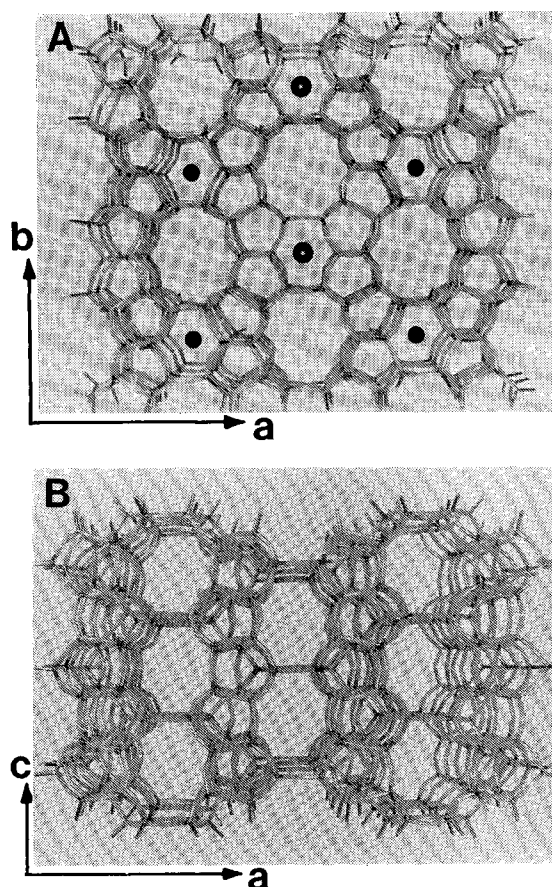

Fig. 1. Structural model of unfaulted ferrierite viewed down [001] (**A**) and [010] (**B**). Solid dots in **A** denote Mg at $z = 0$; open dots $z = 0.5$.

with the same chain topology parallel to [001] as the double-crankshaft building blocks in feldspar structures.

Shear faults. One type of shear fault occurs parallel to (100) planes through the shear of adjacent ferrierite columns or wollastonite chains by $c/2$ (Fig. 3A and 3B). This would produce streaking in SAED patterns perpendicular to c^* and parallel to a^*. When viewed along [010], the shear-faulted portion of the structure places the eight-membered ring channels directly adjacent to one another and transforms the five-membered ring sheet into a sheet composed of alternating four- and six-membered rings. In contrast, the [001] axis view is identical to the unfaulted version. The fact that the shear is constrained by the structure to be increments of $c/2$ means that streaking appears only on the $l = 2n + 1$ rows. Shear faults with a translation of $c/2$ are also possible parallel to (010) planes, but HRTEM evidence of this is difficult to obtain because of the scarcity of [010] views. XRD evidence for both of these faults was obtained for the Lovelock ferrierite (Rice et al., 1994).

Another type of shear fault occurs parallel to {110} and involves a shear of $(a + b)/2$ or $(a - b)/2$ (Sanders, 1985)
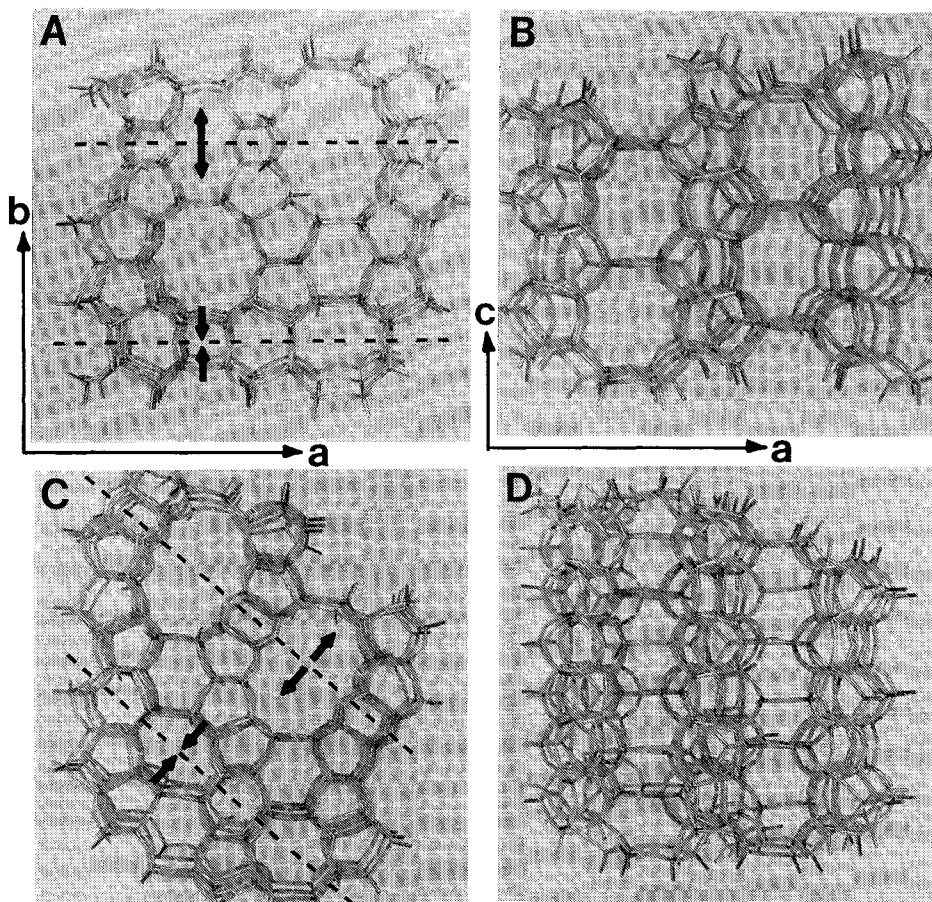
Fig. 2. Structural model of sigma transformations in ferrierite. (A and B) Type (010) viewed down [001] and [010], respectively. (C and D) Type (110) viewed down [001] and [010], respectively. In A and C lower portion of the model is contracted, upper portion expanded. The (010) faults leave the [010] projection unaffected but change ten- and six-membered rings of [001] projection. The (110)-type faults alter ten-membered rings (C), block eight-membered ring channels (D).

(Fig. 3C and 3D). Both of these could occur and intersect within the same crystal and alter its sorption and diffusion properties. The connectivity of the ten-membered rings is disturbed by the fault; instead of alternating six- and eight-membered rings, there are seven-membered rings alternately pointing in opposite directions. Connectivity changes accompanying these planar defects could induce some steric or local framework charge effects.

Kokotailo et al. (1989) described potential faults created by rotation through 90° of adjacent layers parallel to (001) planes. Gramlich-Meier (1986) used double, triple, and quadruple chains to build frameworks related to ferrierite. These theoretical structures are interesting from a topological standpoint but do not appear realistic in view of the observed diffraction patterns for ferrierite.

Methods

An altered olivine basalt from Kamloops Lake, British Columbia, was obtained from Parker Minerals (Livingston, New Jersey). Zeolite occurs in small vugs that are often lined with a chalcedony coating up to 1 mm thick. Clean bundles of lath-shaped crystals were plucked using tweezers and embedded and microtomed following techniques of Csencsits et al. (1985). Sections were estimated on the basis of interference colors to be ~40 nm thick.

Images were obtained on a Philips 420ST, operated at 100 kV at an electron optical magnification of 100000×, after allowing the specimen to desiccate overnight in the microscope vacuum to reduce beam damage rates related to H_2O content. Under these conditions, crystallinity of natural zeolites is preserved only for a few seconds under a condensed electron beam. Thus, care was taken to subject thin sections to as little electron flux as possible, using a Philips Minimum Dose Unit. Microscope imaging conditions (e.g., focus, stigmation, and exposure settings) were established on a region nearby the field of interest, and the field itself was irradiated only during the recording of the micrograph.

Compositional data for zeolite crystals were obtained using energy-dispersive X-ray microanalysis at 200 kV
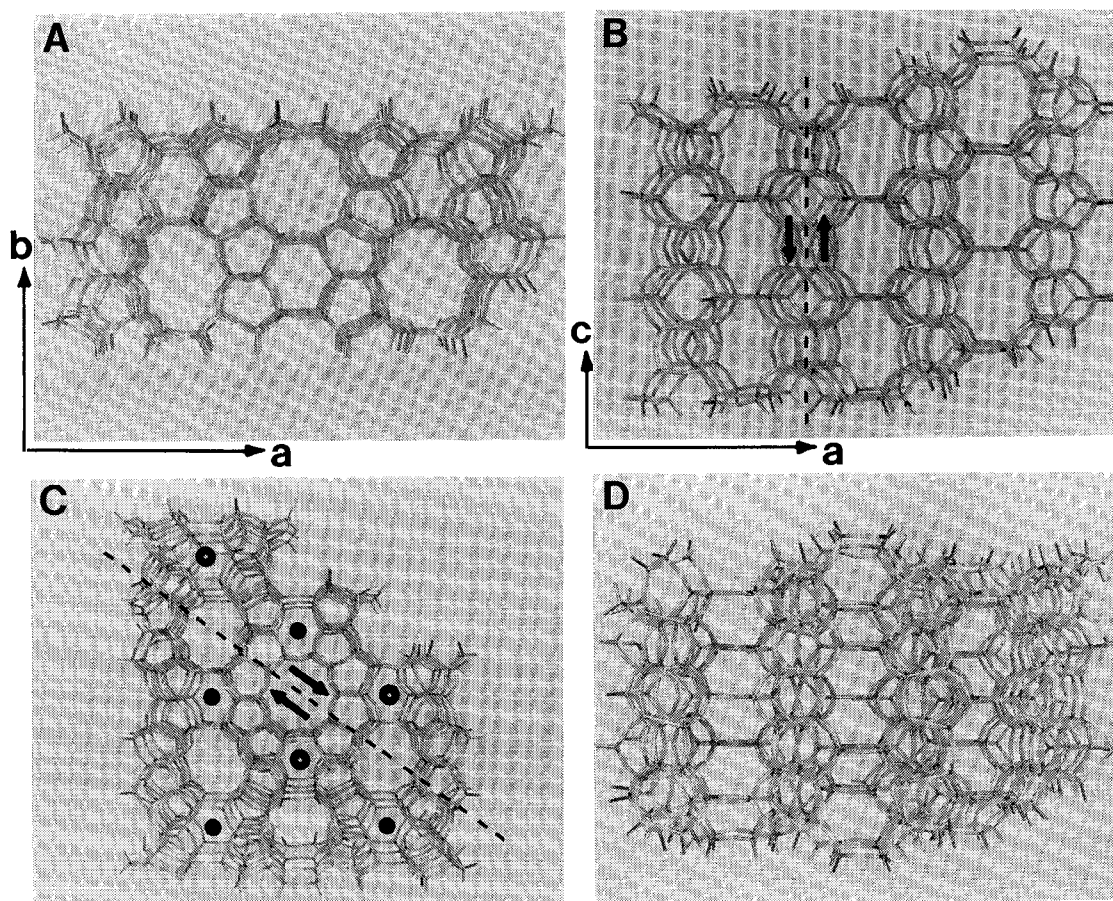
Fig. 3. Structural model of shear-faulted ferrierite. Blocks of ferrierite are shifted along [001] by $c/2$, leaving [001] unaffected (A), but eight-membered ring channels offset by $c/2$ in unfaulted ferrierite (right side of B) are juxtaposed (left side of B). (C and D) An $(a - b)/2$ shear fault viewed down [001] (C) and [010] (D). Solid dots in C denote Mg at $z = 0$; open dots $z = 0.5$. Shear parallel to (110) planes blocks eight-membered ring channels (D).

on a JEOL 2000FX analytical electron microscope and the Cliff-Lorimer thin-film approach (k factors were determined using biotite, hornblende, plagioclase, and orthoclase) (Cliff and Lorimer, 1975).

Image simulations for ferrierite were obtained using the MacTempas multislice program (Kilaas, 1987) available from Total Resolution, Berkeley, California.

RESULTS

HRTEM imaging of ferrierite

Kamloops Lake ferrierite described in this study does not consist of single-crystal fibers. Instead, it consists of several crystallites that share a common c axis but are mostly misaligned in the other crystallographic directions. Crystallite distinction is ambiguous because some crystallites may be faulted portions of others. Figure 4 shows several 10–15 nm crystallites intergrown to produce what typically appears in a scanning electron microscope as a single octagonal crystal. The crystallites themselves tend to approximate octagonal shapes as well.

Crystallites in Figure 4 show variable orientation. The crystallite in the northeast quadrant shows only (200) fringes in the top-right portion, whereas in the lower half the ten-membered ring channels create a newly hexagonal array of white dots. In the area between A and B and along the trace C-D, (200) fringes are offset by ½[200]. These may be ½($a \pm b$) shear faults hypothesized by Sanders (1985). Although the [001] projection for these faults appears very similar to the unfaulted case, the displacement juxtaposes Mg-filled six-membered ring cages across the fault plane, which are at different heights in the unfaulted structure (compare Figs. 1A and 3C). For this reason the image contrast is reversed across the interfaces A-B and C-D in Figure 4. Further support for this conclusion is that the ~56° angle between C-D and the (200) fringes makes C-D consistent with a trace of {110} planes.

Grain E in Figure 4 is closely aligned with [001], but the contrast appears reversed from that near F in Figure 4. Instead of white dots, as there are near F, the contrast at E is best described as dark dots in a white matrix.
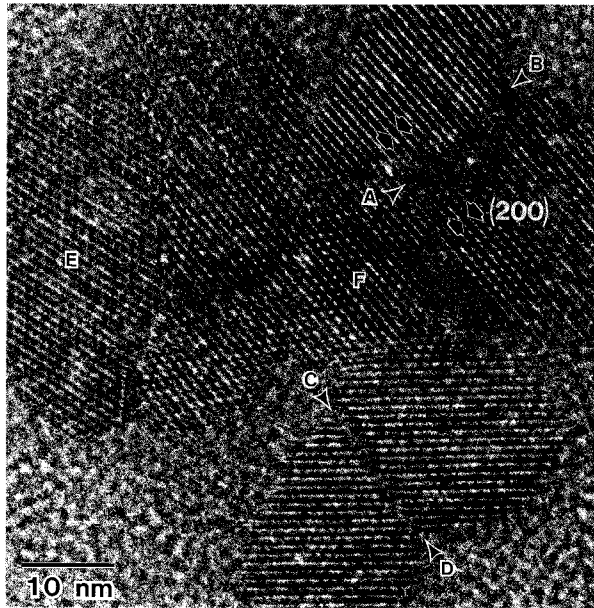
Fig. 4. TEM micrograph of microtomed section of Kamloops Lake ferrierite. On the right, (200) fringes are strong. The interface regions labeled A-B and C-D represent shear-fault boundaries, along which (200) fringes show an apparent shift ½[200]. See text for further explanation.

Figure 5 shows enlarged views of E and F with inset simulated images for comparison. Image simulations of ferrierite approximately parallel to [001] assumed only Si atoms in tetrahedral sites, half the six-membered ring sites filled with Mg cations, and Na cations in the ten-membered ring channels. Because beam damage is a major factor, the homogeneous atomic displacement effects of damage were mimicked by introducing a 0.2 nm mechanical vibration. These calculations indicate that the contrast between areas E and F is not simply reversed. Where there are white dots in a dark matrix (Fig. 5A), the white dots correspond to the ten-membered rings, and where there are dark dots in white matrix (Fig. 5B),
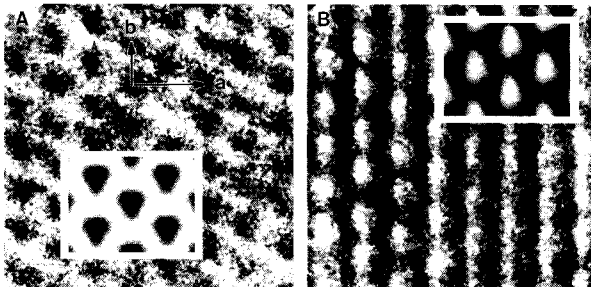

Fig. 5. (A and B) Enlarged view of areas E and F of Fig. 4, respectively, with simulations inset. Thickness 40 nm; defocus −60 nm. In A specimen is tilted 1 mrad about a axis. In B specimen is tilted ∼3 mrad about b axis and 5 mrad about a axis.
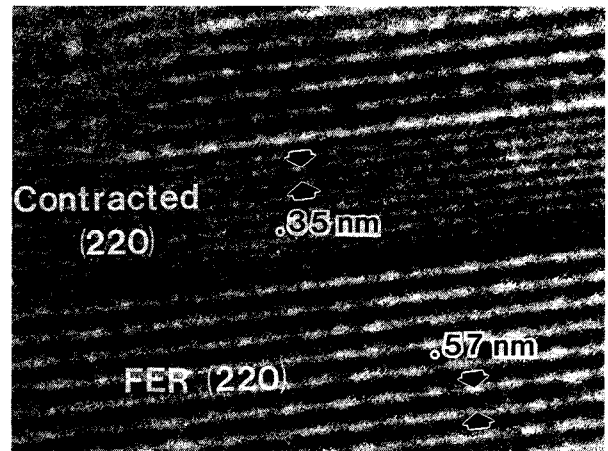

Fig. 6. TEM micrograph of microtomed section of Kamloops Lake ferrierite. Region in middle of micrograph is contracted ∼40%, consistent with a (110)-type contraction fault.

the dark dots correspond to the six-membered ring positions. Simulations are in reasonable agreement with the experimental images, indicating that both crystallites are close to the [001] axis, differing by only several millirads. Subtle changes in crystal orientation and cation contents can result in large differences in the images calculated for ferrierite and must be considered for image simulations of other natural zeolites as well.

Because the Kamloops ferrierite specimen examined here consists of polycrystalline bundles, the question arises whether the structural data of Vaughan (1966) and Kerr (1966) were obtained from single crystals. The refinements may represent an average structure of several small, slightly misoriented crystals, and the crystals may also contain defects. Alberti and Sabelli (1987) refined the structure of a Sardinian ferrierite and obtained posi-
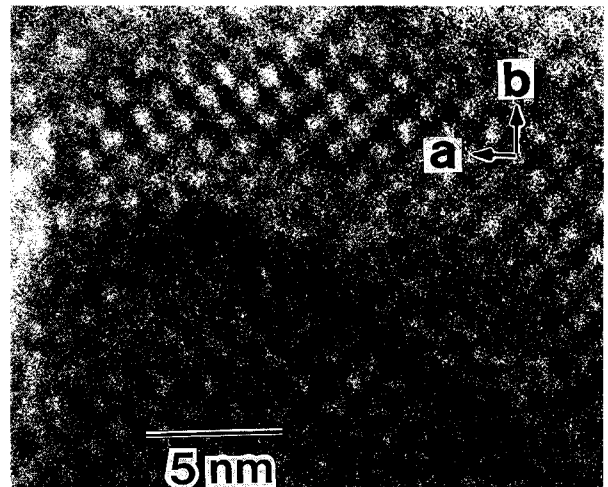

Fig. 7. TEM of crushed grain mount of Kamloops Lake specimen. Mordenite [001] projection.

TABLE 1. Chemical compositions of ferrierite and mordenite (on the basis of 72 and 96 O atoms)

	Kamloops ferrierite (this study)	Kamloops ferrierite (this study)	Kamloops ferrierite (Wise and Tschernich, 1976)	Kamloops mordenite (this study)	Av. mordenite (Gottardi and Galli, 1985)
Si	29.4 ± 1.8	39.2 ± 2.0	30.2 ± 1.8	41.79 ± 2.2	39.67 ± 2.0
Al	6.47 ± 0.4	8.6 ± 0.4	5.81 ± 0.3	8.70 ± 0.5	8.18 ± 0.4
Ti	0.0	0.0	—	0.06 ± 0.01	—
Fe	0.09 ± 0.01	0.12 ± 0.02	0.04 ± 0.01	0.17 ± 0.02	0.17 ± 0.02
Mg	0.79 ± 0.80	1.05 ± 0.10	1.64 ± 0.22	0.15 ± 0.02	0.18 ± 0.02
Ca	1.28 ± 0.12	1.71 ± 0.18	0.07 ± 0.01	2.19 ± 0.22	1.87 ± 0.19
K	0.52 ± 0.05	0.69 ± 0.07	0.35 ± 0.05	0.92 ± 0.95	0.41 ± 0.04
Na	2.30 ± 0.4	3.07 ± 0.38	1.55 ± 0.22	2.64 ± 0.30	3.51 ± 0.36
O	72	96	72	96	96
Si/Al	4.6	4.6	5.2	4.8	4.8

tional parameters and symmetry consistent with previous investigations. It is not known whether their ferrierite consisted of defect-free individual crystals.

The most common planar defect observed in the Kamloops ferrierite involves intergrowths of material with periodicities different from the host periodicity. These intergrowths represent several percent of the crystals imaged in cross section. Figure 6 shows a 3 nm thick intergrowth with an apparent spacing of 0.35 nm compared with the predominant (220) spacing of 0.57 nm. This material is interpreted to be a discrete sigma contraction domain for the following reasons: (1) The viability of this ferrierite contraction on {110} planes was demonstrated by a model construction (shown in the lower half of Fig. 2C) and a distance least-squares (DLS) calculation. (2) The observed fringe spacing is about 40% smaller than the ideal ferrierite (220) spacing, compared with a theoretical contraction of 44% as measured from the [001]-equivalent projection of the DLS model.

It is conceivable that these intergrowths represent another set of planes in the ferrierite structure (d_{040} = 0.353 nm; d_{202} = 0.349 nm) or even another zeolitic phase. Mordenite has several d values close to 0.35 nm (e.g., d_{421} = 0.363 nm; d_{510} = 0.357 nm; d_{022} = 0.353 nm; d_{202} = 0.348 nm; d_{060} = 0.342 nm; and d_{350} = 0.339 nm). However, these would not necessarily intergrow coherently along (220) of ferrierite. The most likely possibility for a coherent intergrowth would be the ferrierite [010] direction mating with the mordenite [100] direction, both of which have eight-membered ring apertures. Not only is the topology too distorted for intergrowth, but there are residual tetrahedral linkages left dangling across phase boundaries. Attempts to construct physical models using tetrahedra and tubing, in which ferrierite and mordenite intergrow coherently across planar boundaries parallel to rational crystal faces, met with failure. Intergrowth models using chain linkages of the type envisioned by Gramlich-Meier (1986) combined with DLS calculations could be fruitful.

Considering the mirror planes normal to **b** and the supposed ease with which sigma faults could occur at these mirror positions, why do (110)-type faults occur instead of (010)-type faults? The reasons may relate to the Mg content of the ferrierite. The Kamloops specimen has a

Mg content of 0.8–1.6 out of a possible 2.0 per unit cell. The (010)-type faults would alter the ferrierite cages and render them less favorable for Mg occupancy because the cages themselves would contract or expand. On the other hand, it is clear from Figure 2 that (110)-type sigma faults do not significantly affect the ferrierite cages, and, consequently, the presence of substantial Mg may stabilize these faults. As with the (010)-type sigma faults, (110)-type faults produce streaking in an SAED pattern, in this case oriented parallel to [110]* for all (00l)* rows.

To evaluate whether microtomy affected sigma faulting, crushed grain mounts were examined for [001] projections because this view best reveals sigma faulting. An extensive search in image and diffraction modes was conducted on ~5000 crystals. One SAED pattern aligned closely with the [001] axis was obtained, and it revealed no evidence of faulting. The lack of [001] views is due largely to the prominent (100) cleavage.

Mordenite in the Kamloops Lake, British Columbia, specimen

The zeolite mordenite occurs in the Kamloops specimen. It was probably not observed in previous work because of its low abundance, and it was observed during this study while searching for ferrierite defects. The spacings between crystallographic planes in Figure 7 are close to a (110)-type sigma expansion hypothesized for ferrierite, but close inspection of d-value ratios reveals that it is mordenite. A thorough SAED examination of the specimen revealed the occasional presence of mordenite. Unit-cell parameters obtained from these patterns are a = 1.80, b = 2.02, and c = 0.752 nm. Chemical compositions in Table 1 were obtained by averaging analyses from several crystals of mordenite and ferrierite.

Just as the Mg occupancy in the ferrierite framework may influence the type of defect that occurs, stability of ferrierite with respect to mordenite relates to the microchemical environment of crystallization. Ferrierite is the only natural zeolite that requires Mg for its formation, as judged from the presence of Mg as a significant constituent in all known natural ferrierite samples (Sameshima, 1986). In the sedimentary ferrierite deposit near Lovelock, Nevada, mordenite is the second most abundant phase (Rice et al., 1992), so the observation of mordenite

in the Kamloops specimen is not surprising. Also, like the Lovelock deposit, the Kamloops ferrierite crystals analyzed in this study are more magnesian than the mordenite. However, the Mg concentration (0.8/unit cell) measured for ferrierite in this specimen is one-half the value reported for another Kamloops specimen by Wise and Tschernich (1976) and lower than that of the monoclinic Altoona ferrierite. I conclude that mordenite cocrystallization was favored by relatively low Mg in the crystallizing fluid in the small pocket represented by this specimen. This is the first report of mordenite from Kamloops, and it underscores the frequent association of these two zeolites worldwide and the need for TEM studies to characterize the fine-scale mineral associations found in many zeolite assemblages.

ACKNOWLEDGMENTS

REFERENCES CITED

Alberti, A., and Sabelli, C. (1987) Statistical and true symmetry of ferrierite: Possible absence of straight T-O-T bridging bonds. Zeitschrift für Kristallographie, 178, 249–256.

Cliff, G., and Lorimer, G.W. (1975) The quantitative analysis of thin specimens. Journal of Microscopy, 103, 203–207.

Csencsits, R., Schooley, C., and Gronsky, R. (1985) An improved method for thin sectioning of particulate catalysts. Journal of Electron Microscopy Technique, 2, 643–644.

Gottardi, G., and Galli, E. (1985) Natural zeolites. In Minerals and Rocks, 18, 409 p.

Graham, R.P.D. (1918) On ferrierite, a new zeolitic mineral from British Columbia; with notes on some other Canadian minerals. Transactions of the Royal Society of Canada Series, 312, 185–201.

Gramlich-Meier, R. (1986) Ancient oriental pattern and related zeolite type networks. Zeitschrift für Kristallographie, 177, 237–245.

Gramlich-Meier, R., Meier, W.M., and Smith, B. (1984) On faults in the framework structure of the zeolite ferrierite. Zeitschrift für Kristallographie, 169, 201–210.

Gramlich-Meier, R., Gramlich, V., and Meier, W.M. (1985) The crystal structure of the monoclinic variety of ferrierite. American Mineralogist, 70, 619–623.

Kerr, I.S. (1966) Structure of ferrierite. Nature, 210, 294.

Kilaas, R. (1987) Interactive software for simulation of high resolution TEM images. Proceedings of the 22nd Annual Conference of the Microbeam Analysis Society, p. 293–300.

Kokotailo, G.T., Fyfe, C.A., Gies, H., and Cox, D.E. (1989) Hypothetical two and three dimensional channel zeolite framework structures. In P.A. Jacobs and R.A. van Santen, Eds., Zeolites: Facts, figures, future, p. 715–729. Elsevier, Amsterdam.

Pluth, J.J., and Smith, J.V. (1990) Crystal structure of boggsite, a new high-silica zeolite with the first three-dimensional channel system bounded by both 12- and 10-rings. American Mineralogist, 75, 501–507.

Rice, S.B., Treacy, M.M.J., and Newsam, J.M. (1990) Defect structures in the zeolite ferrierite as characterized by electron microscopy and powder X-ray diffraction. Eos, 71, 1649.

Rice, S.B., Papke, K.P., and Vaughan, D.E.W. (1992) Chemical controls on ferrierite crystallization during diagenesis of silicic pyroclastic rocks near Lovelock, Nevada. American Mineralogist, 77, 314–328.

Rice, S.B., Treacy, M.M.J., and Newsam, J.M. (1994) Shear faults in Lovelock ferrierite: An X-ray and electron diffraction analysis. Zeolites, 14, 335–343.

Sameshima, T. (1986) Ferrierite from Tapu, Coromandel Peninsula, New Zealand, and a crystal chemical study of known occurrences. Mineralogical Magazine, 50, 63–68.

Sanders, J.V. (1985) Crystallographic faulting in the mordenite group zeolites. Zeolites, 5, 81–90.

Shoemaker, D.P., Robson, H.E., and Broussard, L. (1973) The "sigma transformation" interrelating certain known and hypothetical zeolite structures. In Third International Conference on Molecular Sieves, Proceedings, p. 138–143. American Chemical Society, Zurich.

Smith, B.K. (1986) Variations in the framework structure of the zeolite ferrierite. American Mineralogist, 71, 989–998.

Vaughan, P.A. (1966) The crystal structure of the zeolite ferrierite. Acta Crystallographica, 21, 983–990.

Wise, W.S., and Tschernich, R.W. (1976) Chemical composition of ferrierite. American Mineralogist, 61, 60–66.